

Article

Structural and Magnetic Properties of Ni/C Composites Synthesized from Beet Pulp and Corn Stems

Ihor Bordun ^{1,2,*}, Anna Pidluzhna ¹, Fedir Ivashchyshyn ^{1,2}, Anatoliy Borysiuk ², Dariusz Calus ¹  and Krzysztof Chwastek ^{1,*} 

¹ Faculty of Electrical Engineering, Częstochowa University of Technology, 42-201 Częstochowa, Poland; anna.pidluzhna@pcz.pl (A.P.); fedir.ivashchyshyn@pcz.pl (F.I.); dariusz.calus@pcz.pl (D.C.)

² Department of Ecology and Sustainable Environmental Management, Lviv Polytechnic National University, 79000 Lviv, Ukraine; anatoliy.borysiuk@lnu.edu.ua

* Correspondence: ihor.bordun@pcz.pl (I.B.); krzysztof.chwastek@pcz.pl (K.C.)

Abstract: Nickel/carbon composites were synthesized by the carbonization method with the use of the steam-gas activation technique. Beet pulp and corn stems were used as initial raw materials for composites synthesis. The obtained substances were analyzed by means of scanning electron microscopy, X-ray diffraction analysis, and magnetic properties investigation. The presence of nickel in synthesized composites was estimated during analysis, and the average particle size of nickel was determined as well. The specific surface area of the obtained samples was measured by the technique of Methylene blue sorption from the aqueous solution. The results of the performed investigation demonstrate clearly the promising application of synthesized composites as magneto-active sorbents, which could be easily separated from water solutions.



Citation: Bordun, I.; Pidluzhna, A.; Ivashchyshyn, F.; Borysiuk, A.; Calus, D.; Chwastek, K. Structural and Magnetic Properties of Ni/C Composites Synthesized from Beet Pulp and Corn Stems.

Magnetochemistry **2021**, *7*, 31.

<https://doi.org/10.3390/magnetochemistry7030031>

<https://doi.org/10.3390/magnetochemistry7030031>

Academic Editor: Joan-Josep Suñol

Received: 1 February 2021

Accepted: 23 February 2021

Published: 25 February 2021

Publisher's Note: MDPI stays neutral with regard to jurisdictional claims in published maps and institutional affiliations.



Copyright: © 2021 by the authors. Licensee MDPI, Basel, Switzerland. This article is an open access article distributed under the terms and conditions of the Creative Commons Attribution (CC BY) license (<https://creativecommons.org/licenses/by/4.0/>).

Keywords: metal–carbon composites; X-ray diffraction analysis; magnetic hysteresis; Curie temperature; Ni nanoparticles

1. Introduction

The most popular technologies nowadays are those using water. Food, textile, paper, and many other industries consume large volumes of water resources [1,2]. The world usage of water per day is commensurate with natural resources capacity per year. Such tendency in world industry development is the main reason that water pollution has become a global problem. One of the numerous pollutants is heavy metal ions. They influence human health and the environment strongly even at the trace level [3]. Methods such as chemical deposition, adsorption, coagulation/flocculation, ion exchange, membrane filtering, and electrosorption are typically used for heavy metal extraction from water solutions [4–8]. Adsorption is the most popular method because of the low cost of inputs for sorbents, simplicity, and high efficiency. Moreover, this method is characterized by a low level of secondary pollution.

The key role in the water treatment systems is that played by activated carbon sorbent because of the combination of a developed porous structure and large specific surface area [8]. However, there is a problem of small sorbent particles extraction in the industrial water treatment process. The most promising method for this problem solution is the magnetic separation, which implies that not pure carbon is used, but rather a composite of active carbon with magneto-active materials [9–12]. It is worth mentioning that Fe, Co, or Ni nanoparticles in inert carbon matrixes can be used not only as sorbents but also as magnetic sensors, data recording systems, or catalysts [10,13–16].

The synthesis of the aforementioned composites can be carried out by different methods, but they are quite complex and require expensive reagents in most cases. Moreover, the methods are not environmentally benign [17–21].

Corn is one of the world's major crops, and it is grown in many countries [22]. However, used cobs and stems often do not undergo utilization and become a waste. Considering this fact, many scientists work on the ways of possible utilization procedures of agriculture wastes, and many scientists propose applying corn cobs and stems for the synthesis of highly efficient activated carbon. For example, Martínez-Casillas with co-authors presented a theoretical and experimental study in which they propose applying a residue of corncob gasification as an electrode for supercapacitors [23]. Cao with co-authors propose using an activated carbon synthesized from corn cob as a highly efficient sorbent with a developed surface area [24]. Mishra with colleagues propose applying the corn husk-derived activated carbon for the removal of phenol and para-nitrophenol from aqueous solutions [25]. The beet pulp wastes are the main by-product generated during processing beet sugar, and these wastes can be used for activated carbon synthesis [26] and as efficient sorbents, as it is proposed in work [27].

Therefore, this work is focused on the synthesis of an Ni/carbon (Ni/C) composite from natural beet pulp and corn stem precursors with a simple technique and on the investigation of structural and magnetic properties of synthesized composites.

2. Experiments and Methods

2.1. Sample Preparation

The beet pulp and corn stems were used as an initial raw material, which was washed with the distilled water under room temperature until the filtrate became visually transparent. Then, the washed materials were dried in air atmosphere at 100–110 °C until the constant weight was reached.

The nickel chloride NiCl_2 (anhydrous, powder, 99.99% trace metals basis) purchased from Sigma-Aldrich was used for the synthesis of the Ni/C composite. The dry and milled beet pulp and corn stems were poured over with 1M solution of NiCl_2 with the salt/raw material ratio 1:10 by weight and kept at room temperature for 48 h. Then, the material soaked with the salt was dried at 110 °C until the constant weight was reached. The synthesis of the Ni/C composite was made by the carbonization method with the steam-gas activation technique in the reactor with ultrasound generation of water aerosol in argon (Ar) atmosphere at 700 °C for 90 min. Gaseous by-products were withdrawn out of the reactor with Ar flow through a hydro-seal. The Ar overpressure was kept at the level of 1 kPa and the gas flow rate was in the range 2–10 L/min.

The synthesis of the control carbon material free of Ni ions was made with the same initial raw material under the same conditions but without NiCl_2 to compare the structural properties properly.

As-obtained pure carbon materials and Ni/C composites were boiled three times in distilled water for 30 min every time in boiling flasks with reflux condensers. Then, synthesized materials were dried until the constant weight at 100 °C and milled mechanically in a porcelain mortar. The products of the synthesis were labeled as Activated Carbon Beet 0 (ACB0) and Activated Carbon Corn 0 (ACC0) for pure activated carbons synthesized from beet pulp and corn stems, respectively, and Ni/C composites were labeled as ACB-Ni and ACC-Ni for beet pulp and corn stems initial materials, respectively.

2.2. Methods of Investigation

The scanning electron microscope integrated with low vacuum chamber, and energy-dispersive microanalysis system REMMA-102-02 was used for exploring the morphological properties of synthesized materials. An X-ray diffraction investigation of synthesized materials was made by means of a DRON-3 diffractometer with $\text{CuK}\alpha$ -radiation ($\lambda = 0.1542$ nm) monochromatized by the reflection from the (002) plane of pyrocarbon. The registration of scattered radiation was carried out in the scan mode with a 2°/min scan rate in the angular range of $2\Theta = 5^\circ - 120^\circ$ at room temperature.

The specific surface area analysis was made by the method described in detail in [28], which is based on the sorption of Methylene blue from the aqueous solution by means of

a mono-beam spectrophotometer SF-46 with an integrated microprocessor system. The measurements were done in the cells with an optical path length of 10 mm.

Magnetic measurements were carried out with use of a vibrating-sample magnetometer [29], which was calibrated by the method of comparison with a pure nonporous Ni of density $\rho = 8.9 \text{ g/cm}^3$ as the etalon material. Magnetic hysteresis measurements were performed within the +300 to -300 kA/m magnetic field range. The amount of magneto-active phase in synthesized products was determined according to specific saturation magnetization data. High-temperature measurements of magnetic properties were carried out in a micro-oven placed in the working gap of the electromagnet [29]. The coils at the poles of electromagnet, placed in water-cooling holders, were cooled by running water. The investigated composites were placed in a cylindrical titanium container of 4–5 mm diameter, the lid of which served as a punch while pressing the material with the necessary effort in the container. The magnetic moment of the container was subtracted from the magnetic moment of the powder with the container. The temperature of the sample was controlled by chromel-copel (cupronickel) or platinum–rhodium–platinum thermocouples (type L and type R by IEC 60584-1,2). The inspection of the measured temperature was carried out by measuring the Curie temperature of pure nickel.

Under measurements in magnetic fields of insufficient magnetic intensity, the measured magnetization is not a single-valued function of ferromagnetic phase in a sample. It depends also on the structure of the phase, dispersivity, stresses, sample history, etc. Therefore, the quantitative measurements of saturation magnetization in phase analysis have to be done under magnetic fields strong enough for complete saturation. The problem of valid measurements for saturation magnetization becomes even more complicated when it should be done for ferromagnetic particles in a nonmagnetic matrix as it is for the Ni/C composite. The influence of the demagnetization factor for particles is essential in this case, and the application of intensive fields enables one to get the reliable data. Therefore, the specific saturation magnetization and its temperature dependence were measured under a magnetic field of 800 kA/m intensity in this work.

3. Results and Discussion

SEM images of the synthesized carbons and Ni/C composites are presented in Figure 1a–d. The synthesized substances are mostly carbon-based materials, but there are inclusions of some other phases. The X-ray investigation confirmed that this phase is quartz. Most probably, and as it sometimes happens, the presence of small amounts of silica could be explained by the micro-destructions in ceramic mortar during mechanical milling [30].

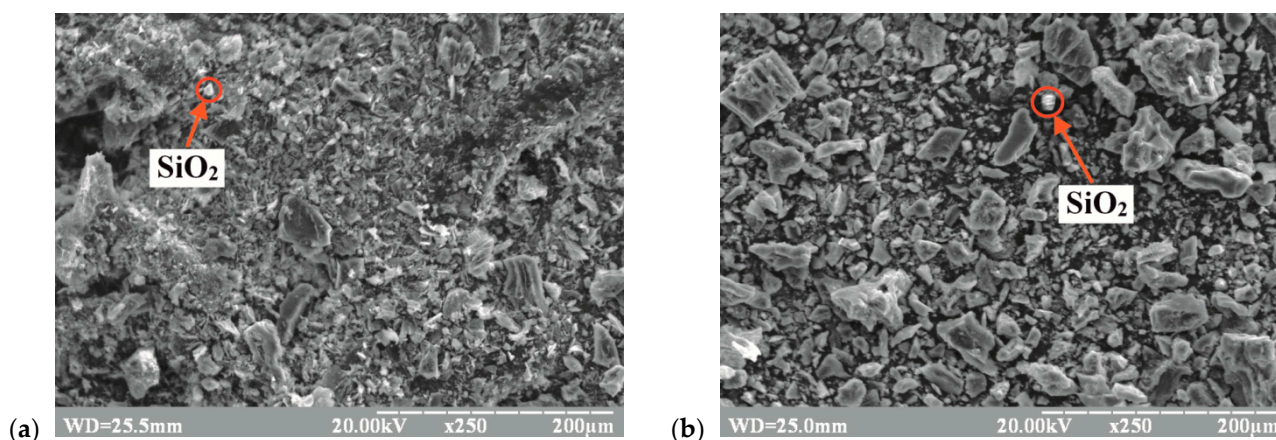


Figure 1. Cont.

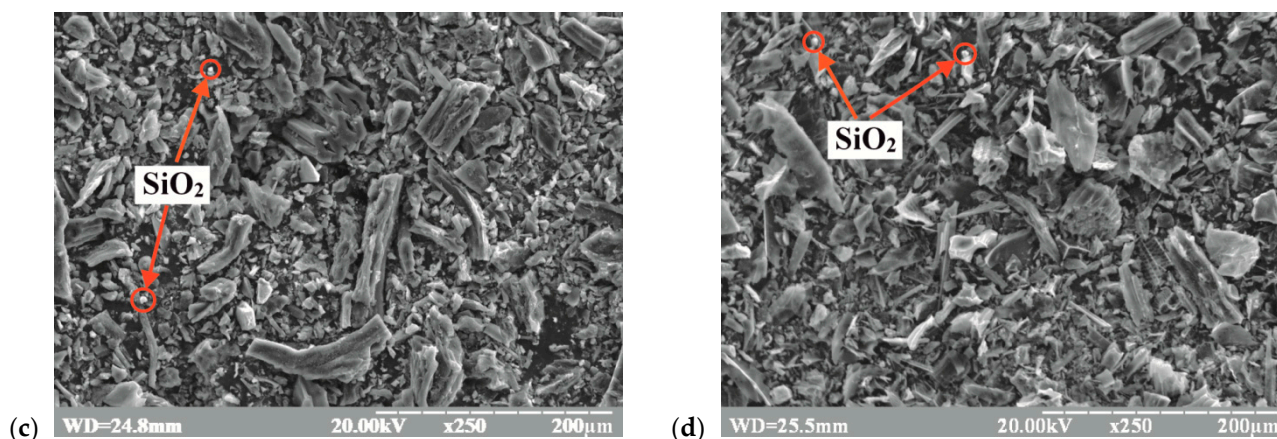


Figure 1. SEM images of ACB0 (a), ACC0 (c) carbons, ACB-Ni (b), and ACC-Ni (d) Ni/C composites.

X-ray diffraction data collected for synthesized samples are presented in Figure 2. The XRD patterns reveal the presence in investigated samples of two phases, and these are mainly amorphous carbon and Ni. The two sharp and well-defined peaks at $2\Theta = 20.8^\circ$, 26.6° correspond to the diffraction on the (100) and (101) crystal planes of quartz, respectively [31–34]. As it was already mentioned, the presence of small amounts of silica could be explained by the micro-destructions in ceramic mortar during mechanical milling [30]. The two distinct diffraction peaks at $2\Theta = 44.5^\circ$, 51.5° as seen in Figure 2a, for samples ACB-Ni and ACC-Ni, belong to face-centered cubic Ni and correspond to the (111) and (200) crystal planes of nickel [30,35–38]. No diffraction peaks of other impurities are observed, confirming the successful formation of the Ni/C magnetic composites. Significantly, there are no maxima for Ni oxides in the patterns for ACB-Ni and ACC-Ni samples, confirming the complete reduction of Ni by carbon during the carbonization reaction under the applied conditions. The nickel phase proves itself with distinct characteristic peaks, suggesting its high crystallite level [36]. All samples demonstrate one broad weak diffraction peak at 2Θ around 24° corresponding to the diffraction on carbon layers for amorphous carbon [39]. According to the calculated results from the 002 diffraction peaks based on the Bragg equation, the interlayer distance d of ACB0, ACB-Ni, ACC0, and ACC-Ni are 0.374, 0.375, 0.371, and 0.374 nm, respectively. It could be mentioned that there is a slight decrease in interlayer distance of Ni/C composites ACB-Ni and ACC-Ni compared to Ni-free carbon samples ACB0 and ACC0.

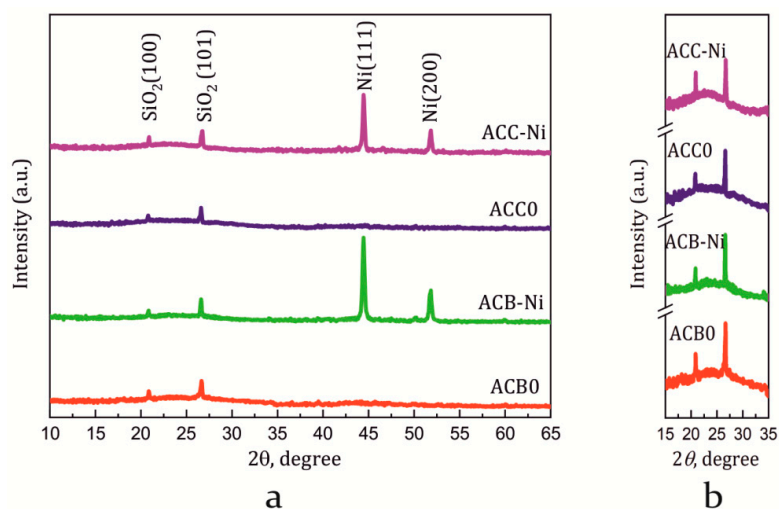


Figure 2. XRD patterns of pure carbons (ACB0, ACC0) and Ni/C magnetic composites (ACB-Ni, ACC-Ni) (a), and zoom-in view (b).

The values of specific surface area for synthesized materials, estimated from the sorption method [28], are 91 and 187 m²/g for ACB0 and ACC0 samples, respectively and 138 and 325 m²/g for ACB-Ni and ACC-Ni samples, respectively. It is a well-known fact that the addition of salts of iron to the initial raw material during the carbonization procedure induces the development of porosity and specific surface area [27,40]. The results of the present work show that the salt of Ni causes the development of a specific surface area in synthesized composites to some extent as well.

Figure 3 shows σ - H loops for Ni/C composites, where σ is specific magnetization and H is magnetic field intensity. A comparative analysis of the magnetic properties for synthesized samples attests that the specific magnetization value of the ACB-Ni sample is twice as much as the specific magnetization value of the ACC-Ni sample. In addition, the estimated values of specific saturation magnetization σ_s are twice as much as magnetizations of studied in previous work [27] featuring Fe/carbon composites, where the Fe₃O₄ was the source of the magnetic moment.

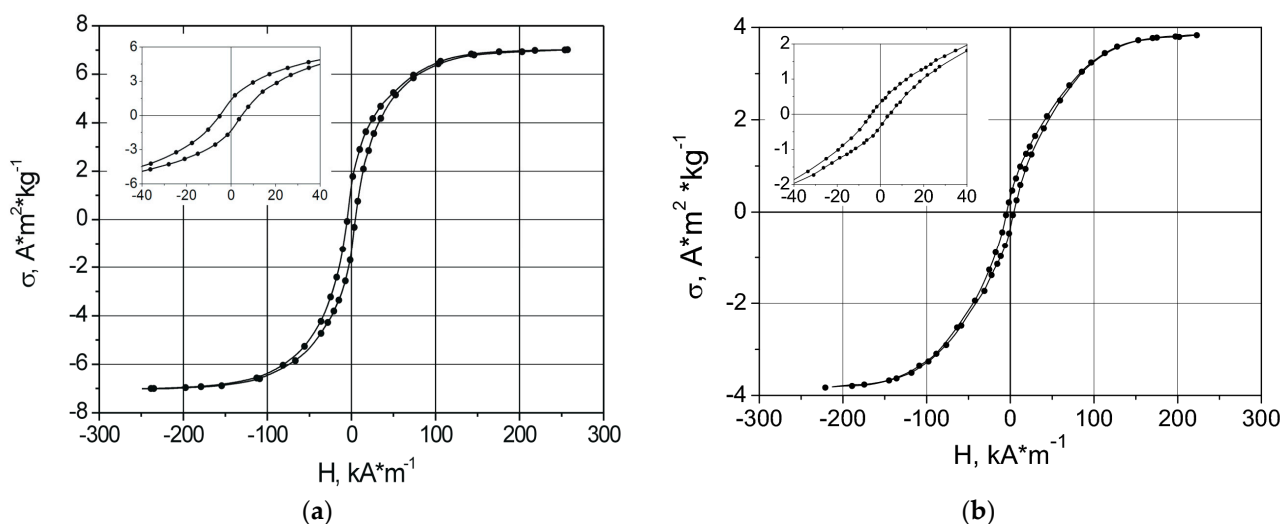


Figure 3. σ - H loops for Ni/C composites ACB-Ni (a) and ACC-Ni (b). The region of the low magnetic field is shown in the inset.

Higher values of coercive force H_c for the ACB-Ni sample are obviously caused by the higher degree of dispersion of Ni particles as magnetic moment carriers in investigated composites.

The evaluation of size for Ni particles in samples synthesized in the present work was carried out, following the methodology presented in Ref. [41]. The average particle size of Ni for the sample ACB-Ni was 80 nm, whereas it was 100 nm for the sample ACC-Ni. The authors of Ref. [42] mention that the critical transition radius to a single-domain state of Ni nanoparticles at 300 K is 85 nm, and the critical transition radius to a superparamagnetic state is 30 nm. However, the low values of coercive force (see Table 1) indicate the excess of Ni nanoparticle size in synthesized composites over a single-domain critical value.

Table 1. Magnetic properties of synthesized Ni/C composites.

Sample	σ_s , A·m ² /kg	H_c , kA/m	Ni, wt. %
ACB-Ni	7.1	5	13
ACC-Ni	3.9	4	7.2

Phase magnetic analysis made by saturation magnetization measurements at different temperatures under saturating fields revealed (see Figure 4) the presence of one ferromagnetic phase with a Curie temperature near 345 °C in synthesized composites. The Curie temperature for the bulk of Ni is 358 °C according to Ref. [43]. Apparently, the temperature difference for magnetic transition is caused by the dispersion of Ni particles as magnetic

moment carriers [41,44] in investigated composites and by Ni–carbon interaction with supersaturated solid solution formation through carbon dissolution in Ni.

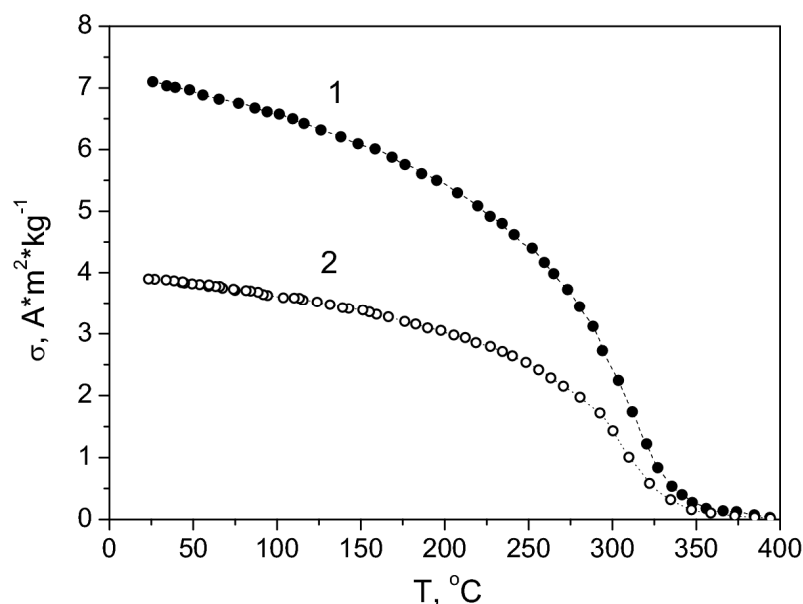


Figure 4. Temperature behavior of specific saturation magnetization for the samples ACB-Ni (1) and ACC-Ni (2) measured at a magnetic field intensity of 800 kA/m.

The determination of specific saturation magnetization enabled us to calculate the content of Ni nanoparticles in synthesized composites (Table 1). Since the significant decrease in magnetization was observed for Ni particles of radii $r \leq 50$ nm [45], the value for specific saturation magnetization for bulk material was used in calculation.

4. Conclusions

The nanostructured Ni/C composites were successfully synthesized from such initial raw materials as beet pulp and corn stems by the carbonization method with use of the steam-gas activation technique.

The X-ray diffraction analysis revealed the presence of metallic Ni in the composites and magnetic measurements, which confirmed the fact that Ni is contained in a porous carbon matrix in the nanoparticle state. The average particle size of Ni nanoparticles was estimated using the dependence of coercive force of particles versus their size. It was determined that for the ACB-Ni sample, the average particle size was 80 nm, and for the ACC-Ni sample, it was 100 nm. The temperature measurements for specific saturation magnetization registered the lower values of Curie temperature for investigated samples if compared with bulk nickel because of the interaction between carbon and Ni nanoparticles and the formation of supersaturated solid solution of carbon in Ni.

The specific surface area was evaluated for synthesized composites, and it is 138 m²/g for the sample synthesized from beet pulp and 352 m²/g for the sample synthesized from corn stems. These values could be increased if the method of composite synthesis is worked out and optimized. Ni salts provide the carbons with magnetic moment carriers and promote the surface development of carbon materials and decrease in impurities content in composites, which are present in initial raw materials. Specific magnetizations for synthesized composites were determined. They were 7.1 and 3.9 A*m²/kg for the samples synthesized from beet pulp and corn stems, respectively, which makes these composites very promising for application as magneto-active sorbents that could be easily separated from water solution.

Author Contributions: Conceptualization, I.B. and A.B.; methodology, A.P. and F.I.; validation, D.C.; formal analysis, K.C.; investigation, I.B. and A.B.; data curation, A.B. and K.C.; writing—original draft preparation, I.B.; writing—review and editing, F.I., A.P. and D.C.; visualization, I.B.; supervision, I.B. and F.I.; project administration, D.C. and K.C.; funding acquisition, D.C. and K.C. All authors have read and agreed to the published version of the manuscript.

Funding: This research received no external funding.

Conflicts of Interest: The authors declare no conflict of interest.

References

1. Jin, Y.; Berhrens, P.; Tukker, A.; Scherer, L. Water use of electricity technologies: A global meta-analysis. *Renew. Sustain. Energy Rev.* **2019**, *115*, 109391. [CrossRef]
2. Gupta, A.D.; Pandey, P.; Feijoo, A.; Yaseen, Z.M.; Bokde, N.D. Smart Water Technology for Efficient Water Resource Management: A Review. *Energies* **2020**, *13*, 6268. [CrossRef]
3. Nriagu, J.O. Global Metal Pollution: Poisoning the Biosphere? *Environ. Sci. Policy Sustain. Dev.* **1990**, *32*, 7–33. [CrossRef]
4. Chen, L.; Sheng, H.L. Electrocoagulation of chemical mechanical polishing (CMP) wastewater from semiconductor fabrication. *Chem. Eng. J.* **2003**, *95*, 205–211. [CrossRef]
5. Ding, Z.H.; Hu, X.; Wan, Y.S.; Wang, S.S.; Gao, B. Removal of lead, copper, cadmium, zinc, and nickel from aqueous solutions by alkali-modified biochar: Batch and column tests. *J. Ind. Eng. Chem.* **2016**, *33*, 239–245. [CrossRef]
6. Huang, C.J.; Yang, B.M.; Chen, K.S.; Chang, C.C.; Kao, C.M. Application of membrane technology on semiconductor wastewater reclamation: A pilot-scale study. *Desalination* **2011**, *278*, 203–210. [CrossRef]
7. Dehkoda, A.M.; Ellis, N.; Gyenge, E. Electrosorption on activated biochar: Effect of thermo-chemical activation treatment on the electric double layer capacitance. *J. Appl. Electrochem.* **2014**, *44*, 141–157. [CrossRef]
8. Bolisetty, S.; Peydayesh, M.; Mezzenga, R. Sustainable technologies for water purification from heavy metals: Review and analysis. *Chem. Soc. Rev.* **2019**, *48*, 463–487. [CrossRef]
9. Safarik, I.; Horska, K.; Pospiskova, K.; Safarikova, M. Magnetically Responsive Activated Carbons for Bio- and Environmental Applications. *Int. Rev. Chem. Eng.* **2012**, *4*, 346–352.
10. Ni, Y.; Jin, L.; Zhang, L.; Hong, J. Honeycomb-like Ni@C composite nanostructures: Synthesis, properties and applications in the detection of glucose and the removal of heavy-metal ions. *J. Mater. Chem.* **2010**, *20*, 6430–6436. [CrossRef]
11. Gymes-Pastora, J.; Brindas, E.; Ortiz, I. Recent progress and future challenges on the use of high performance magnetic nano-adsorbents in environmental applications. *Chem. Eng. J.* **2014**, *256*, 187–204. [CrossRef]
12. Speltini, A.; Sturini, M.; Maraschi, F.; Profumo, A. Recent trends in the application of the newest carbonaceous materials for magnetic solid-phase extraction of environmental pollutants. *Trends Environ. Anal. Chem.* **2016**, *10*, 11–23. [CrossRef]
13. Yu, M.; Liu, Y.; Sellmyer, D.J. Nanostructure and magnetic properties of composite Co Pt: C films for extremely high-density recording. *J. Appl. Phys.* **2000**, *87*, 6959–6961. [CrossRef]
14. Wang, Y.; Wang, J.; Fan, G.; Li, F. Synthesis of novel Ni/C catalyst derived from a composite precursor for hydrodechlorination. *Catal. Commun.* **2012**, *19*, 56–60. [CrossRef]
15. Lyu, S.; Liu, C.; Wang, G.; Zhang, Y.; Li, J.; Wang, L. Structural evolution of carbon in an Fe@C catalyst during the Fischer-Tropsch synthesis reaction. *Catal. Sci. Technol.* **2019**, *9*, 1013–1020. [CrossRef]
16. Aluha, J.; Abatzoglou, N. Gold-promoted plasma-synthesized Ni-Co-Fe/C catalyst for Fischer-Tropsch synthesis. *Gold Bull.* **2017**, *50*, 147–162. [CrossRef]
17. Podsiadły, M.; Narkiewicz, U.; Arabczyk, W. Preparation of carbon-encapsulated cobalt nanoparticles by catalytic ethane decomposition. *Mater. Sci. Poland.* **2008**, *26*, 357–364.
18. Yao, T.; Cui, T.; Wu, J. Preparation of acid-resistant core/shell Fe₃O₄/C materials and their use as catalyst supports. *Carbon* **2012**, *50*, 2287–2295. [CrossRef]
19. Xia, W.; Zou, R.Q.; An, L.; Xia, D.G.; Guo, S.J. A metal-organic framework route to in situ encapsulation of Co@Co₃O₄@C core@bshell nanoparticles into a highly ordered porous carbon matrix for oxygen reduction. *Energy Environ. Sci.* **2015**, *8*, 568–576. [CrossRef]
20. Yan, P.; Guo, W.; Liang, Z.; Meng, W.; Yin, Z.; Li, S.; Li, M.; Zhang, M.; Yan, J.; Xiao, D.; et al. Highly efficient K-Fe/C catalysts derived from metal-organic frameworks towards ammonia synthesis. *Nano Res.* **2019**, *12*, 2341–2347. [CrossRef]
21. Ziogas, P.; Bourlinos, A.B.; Tucek, J.; Malina, O.; Douvalis, A.P. Novel Magnetic Nanohybrids: From Iron Oxide to Iron Carbide Nanoparticles Grown on Nanodiamonds. *Magnechemistry* **2020**, *6*, 73. [CrossRef]
22. Available online: <https://www.statista.com/statistics/254292/global-corn-production-by-country> (accessed on 20 February 2021).
23. Martínez-Casillas, D.C.; Mascorro-Gutiérrez, I.; Betancourt-Mendiola, M.L.; Palestino, G.; Quiroga-González, E.; Pascoe-Sussoni, J.E.; Guillén-López, A.; Muñoz, J.; Cuentas-Gallegos, A.K. Residue of Corn cob Gasification as Electrode of Supercapacitors: An Experimental and Theoretical Study. *Waste Biomass Valor* **2020**. [CrossRef]
24. Cao, Q.; Xie, K.; Lv, Y.; Bao, W. Process effects on activated carbon with large specific surface area from corn cob. *Bioresour. Technol.* **2006**, *97*, 110–115. [CrossRef] [PubMed]

25. Mishra, S.; Yadav, S.S.; Rawat, S.; Singh, J.; Koduru, J.R. Corn husk derived magnetized activated carbon for the removal of phenol and para-nitrophenol from aqueous solution: Interaction mechanism, insights on adsorbent characteristics, and isothermal, kinetic and thermodynamic properties. *J. Environ. Manag.* **2019**, *246*, 362–373. [CrossRef] [PubMed]
26. Bordun, I.; Ptashnyk, V.; Sadova, M.; Chapovska, R. Utilization of sugar beet pulp by getting activated carbon. *Environ. Probl.* **2017**, *2*, 29–32. Available online: <http://science.lpnu.ua/sites/default/files/journal-paper/2017/oct/6412/fulltext.pdf> (accessed on 20 February 2021).
27. Soloviy, C.; Malovanyy, M.; Bordun, I.; Ivashchysyn, F.; Borysiuk, A.; Kulyk, Y. Structural, magnetic and adsorption characteristics of magnetically susceptible carbon sorbents based on natural raw materials. *J. Water Land Dev.* **2020**, *47*, 160–168. [CrossRef]
28. Bordun, I.; Sadova, M.; Gorodnia, T. Determination of the specific surface area of activated carbon materials on the basis of methylene blue adsorption. *Slovak Int. Sci. J.* **2017**, *11*, 17–21. (In Ukrainian)
29. Duriagina, Z.A.; Goliaka, R.L.; Borysiuk, A.K. The Automated Wide-Range Magnetometer for the Magnetic Phase Analysis of Alloys: Development and Application. *Uspekhi Fiziki Metallov.* **2013**, *14*, 33–66. (In Ukrainian) [CrossRef]
30. Galaburda, M.V.; Bogatyrov, V.M.; Tomaszewski, W.; Oranska, O.I.; Borysenko, M.V.; Skubiszewska-Zięba, J.; Gun'ko, V.M. Adsorption/desorption of explosives on Ni-, Co-, and NiCo-carbon composites: Application in solid phase extraction. *Colloids Surf. A* **2017**, *529*, 950–958. [CrossRef]
31. Marinoni, N.; Broekmans, M.A.T.M. Microstructure of selected aggregate quartz by XRD, and a critical review of the crystallinity index. *Cem. Concr. Res.* **2013**, *54*, 215–225. [CrossRef]
32. Jiang, X.; Chen, J.; Wei, M.; Li, F.; Ban, B.; Li, J. Effect of impurity content difference between quartz particles on flotation behavior and its mechanism. *Powder Technol.* **2020**, *375*, 504–512. [CrossRef]
33. Bocullo, V.; Vitola, L.; Vaiciukyniene, D.; Kantautas, A.; Bajare, D. The influence of the SiO₂/Na₂O ratio on the low calcium alkali activated binder based on fly ash. *Mater. Chem. Phys.* **2021**, *258*, 123846. [CrossRef]
34. Adewunmi, A.A.; Amao, A.O.; Kamal, M.S.; Solling, T.I. Demulsification and breaking mechanism of variable quartz concentrates obtained from sand. *J. Pet. Sci. Eng.* **2020**, *192*, 107263. [CrossRef]
35. Li, H.; He, Y.; Yang, Q.; Wang, J.; Yan, S.; Chen, C.; Chen, J. Urchin-like Ni@N-doped carbon composites with Ni nanoparticles encapsulated in N-doped carbon nanotubes as high-efficient electrocatalyst for oxygen evolution reaction. *J. Solid State Chem.* **2019**, *278*, 120843. [CrossRef]
36. Raimundo, R.A.; Silva, V.D.; Simões, T.A.; Medeiros, E.S.; Macedo, D.A.; Morales, M.A. Ni/NiO-carbon composite fibers prepared by solution blow spinning: Structure and magnetic properties. *Ceram. Int.* **2020**, *46*, 18933–18939. [CrossRef]
37. Ying, T.; Zhang, J.; Liu, X.; Yu, J.; Yu, J.; Zhang, X. Corn cob-derived hierarchical porous carbon/Ni composites for microwave absorbing application. *J. Alloys Compd.* **2020**, *849*, 156662. [CrossRef]
38. Ren, H.; Shu, X.; Liu, Z.; Zhou, J.; Ma, J.; Liu, Y.; Kong, L.B.; Min, F.; Shi, X.; Han, J.; et al. In-situ synthesis of layered porous coal-derived carbon/Ni magnetic composites with promising microwave absorption performance. *J. Magn. Magn. Mater.* **2020**, *513*, 167231. [CrossRef]
39. Xiao, N.; Zhang, X.; Liu, C.; Wang, Y.; Li, H.; Qiu, J. Coal-based carbon anodes for highperformance potassium-ion batteries. *Carbon* **2019**, *147*, 574–581. [CrossRef]
40. Zhu, X.; Qian, F.; Liu, Y.; Matera, D.; Wu, G.; Zhang, S.; Chen, J. Controllable synthesis of magnetic carbon composites with high porosity and strong acid resistance from hydrochar for efficient removal of organic pollutants: An overlooked influence. *Carbon* **2016**, *99*, 338–347. [CrossRef]
41. He, X.; Zhong, W.; Au, C.-T.; Du, Y. Size dependence of the magnetic properties of Ni nanoparticles prepared by thermal decomposition method. *Nanoscale Res. Lett.* **2013**, *8*, 446. [CrossRef] [PubMed]
42. Krishnan, K.M.; Pakhomov, A.B.; Bao, Y.; Blomqvist, P.; Chun, Y.; Gonzales, M.; Roberts, B.K. Nanomagnetism and spin electronics: Materials, microstructure and novel properties. *J. Mater. Sci.* **2006**, *41*, 793–815. [CrossRef]
43. Coey, J.M.D. *Magnetism and Magnetic Materials*; Cambridge University Press: Cambridge, UK, 2010; p. 625. [CrossRef]
44. Du, Y.; Xu, M.; Wu, J.; Shi, Y.; Lu, H.; Xue, R. Magnetic properties of ultrafine nickel particles. *J. Appl. Phys.* **1991**, *70*, 5903–5905. [CrossRef]
45. Yao, Y.D.; Chen, Y.Y.; Hsu, C.M.; Lin, H.M.; Tung, C.Y.; Tai, M.F.; Suo, C.T. Thermal and magnetic studies of nanocrystalline Ni. *Nanostruct. Mat.* **1995**, *6*, 933–936. [CrossRef]